In shorter form in MICCAI 1998 proceedings
LNCS 1496: 832-841

BIWI-TR-183 **May 1998**

Motion measurements in low-contrast X-ray imagery[1]

Martin Berger and Guido Gerig

Swiss Federal Institute of Technology
Communication Technology Lab, Image Science
8092 Zürich, Switzerland

{berger,gerig}@vision.ee.ethz.ch

[1] This report has been accepted in shorter form to MICCAI '98.

Abstract

Measuring motion in medical imagery becomes more and more important, in particular for object tracking, image registration, and local displacement measurements. Often, the requirements on the measurement precision are high compared to the image quality. Especially in megavoltage X-ray images (*portal images*), which are used to control the position of patients in high precision radiotherapy, render low contrast, blur, and noise accurate measurements difficult.

In this work we review the framework of a generic matching algorithm only based on the image signal and not on binary image features. Thus, the often unreliable step of feature extraction in such imagery is circumvented. Another major advantage is the possibility of self-diagnosis, which is used for restricting the transformation in motion measurements if the image quality is not sufficient.

The matching leads to an estimate of parts of the rigid 3D motion of the patient during radiotherapy, based on the measurements in the projected 2D portal images. The method of digitally reconstructed radiographs (DRR) allow for the computation of error free reference images, avoiding the additional step of therapy simulation. The multi-modal match between such DRRs and portal images lead to an estimate of the patient position during radiotherapy treatment. Results of generated data with known ground truth as well as results of a multi-modal match are presented.

Keywords — portal imaging, medical image analysis, image matching, deformable templates, self-diagnostics

1 Introduction

Accurate motion measurements in images are essential to solve numerous problems in computer vision. For medical imagery in particular, precise position measurements and registration of image series represent two important applications. Wherever feature extraction is difficult or high precision is required, the least squares template matching algorithm (LSM) reviewed in this paper has many advantages over other methods. LSM is a generic matching algorithm suitable for many applications including motion estimation in low-contrast megavoltage X-ray images, also called *portal images*.

The specific goal in this work is the exact positioning of patients during radiotherapy, which is essential for high precision treatment. This involves automatically measuring patient setup deviation between or even during treatment sessions. One possible sensor is an electronic portal imaging device (EPID), which delivers images of the exit dose distribution during treatment. Unfortunately, the contrast of these megavoltage X-ray images is very low due to the high energy beam, and, since we are dealing with projected images, parts of a rigid 3D motion must be estimated by evaluating projected 2D images. Thus, the quantitative processing of portal images is a very challenging task.

In [Berger and Danuser 1997] we propose the area-based LSM algorithm to find displacements between two portal images, yielding a fast and accurate image matching procedure. Extending this approach, we further exploit the self-diagnosis capabilities. The variation of image quality of portal images inhibits the estimation of a 2D affine transformation for all cases. An adaptive scheme based on self-diagnostic measures allows for an automatic reduction of the parameter set where the full parameter set is not determinable. Furthermore we include the multi-modal matching of portal images against digitally reconstructed radiographs computed from the CT volume data.

1.1 Previous work on portal images

Several methods for portal images matching have been proposed but most are lacking either the robustness or the accuracy necessary to be reliably used in daily hospital routine. Furthermore, they often require too much user interaction. Algorithms like point-to-point (or landmark) matching greatly depend on the exact localization of the landmarks by the physician. This is not only time-consuming, but also varies for different operators. Less user interaction is required by the chamfer matching algorithm where significant ridges are manually outlined in a reference image and matched onto the detected features of the treatment image [Gilhuijs and van Herk 1993]. A similar approach in the sense that it also uses binary features, namely cores, is described in [Fritsch *et al.* 1995], where also a quite complete review about published algorithms for portal imaging can be found.

Since portal images are inherently noisy and low in contrast, it is difficult to robustly detect features like edges, ridges or cores. Therefore, an area-based match is superior to a feature-based algorithm. Greyvalue correlation techniques are described in [Dong and Boyer 1996, Moseley and Munro 1994, Radcliffe *et al.* 1994]. Their limitations lie in the restriction to a translation or in a coarse search grid for computational reasons.

1.2 Previous work on least squares template matching

The method of least squares template matching (LSM) with deformable templates meets the requirements of being an area-based approach with rigorous error propagation, self-diagnosis and thus, minimized user interaction. Early work in this field was presented by [Lucas and Kanade 1981], who published an iterative image registration scheme base on LSM. Among the first papers that discussed the concept of exploiting the full information of the statistical models

for robust template matching are [Grün 1985] and [Förstner 1987]. [Bergen *et al.* 1992] describe basically the same algorithm for motion estimation. It was further developed using a multi-scale approach by [Lindeberg 1995].

Following and extending the original work of Grün, [Danuser and Mazza 1996] achieved highly accurate results at the resolution limit of a light microscope. The high accuracy of this technique even in the case of low-contrast imagery is extensively exploited in [Danuser 1996]. The paper reports of high accuracy positional measurements of a calibration grid used to calibrate a stereo light microscope. Compared to their application, additional problems arise in portal images from the higher complexity of the image scene and the out-of-plane rotations. On the other hand, the requirements on accuracy are not as high in portal imaging.

A similar technique for the registration of medical image series is reported by [Unser *et al.* 1995], where each image is matched to the reference image based on a global greyvalue difference measure. In contrast to their work, our framework does not rely on one global template, but on several small templates each containing a significant image structure. Thus, the inclusion of distinct but insignificant image features which vary between the data of one sequence is avoided and the impact of global greyvalue errors such as bias fields is reduced.

2 Least squares template matching

LSM is an area-based matching algorithm. It replaces the conventional multi-stage approach where feature detection is followed by thresholding, binarization and a discrete search. Thus, LSM does not depend on the extraction of binary (also called *non-iconic*) image features. This is a very important advantage in low-contrast and blurred imagery, where feature detection is mostly unreliable. Furthermore, unlike in most correlation methods, the optimum transformation is not searched by testing all possible cases, but approached using an optimization scheme. Assuming that a fair initial guess can be supplied, this is not only faster but also more accurate.

The image signal of a template is fitted into the search image, minimizing the least squares error between the greyvalues of the two regions. The fitting procedure has to account for both radiometric and geometric transformations. In order to avoid ambiguities, these two transformations have to be estimated separately. This is achieved by estimating the parameters for the radiometric transformation based on a global measure within the template region before each iteration. Thus, they are not directly included in the actual least squares optimization.

The following sections give a short review over the mathematical framework of LSM. Further information can be found in [Berger 1998, Berger and Danuser 1997].

2.1 Unconstrained LSM

The LSM includes two observations, the template image $f[.]$ and the search image $g[.]$, called patch. The geometric relation between the original template and the matched area is defined by an arbitrary transformation. Depending on the type of the chosen transformation, this allows for displacement, rotation and/or deformation of the template. In addition to the geometric transformation, the observations must be adjusted radiometrically. The simultaneous estimation of both types of transformations would lead to an overdetermined system, since it is not possible to distinguish them locally (cf. figure 1). In order to overcome this problem, the parameters of the radiometric transformation are estimated based on a global measure within the template region apart from the actual least squares optimization. The resulting radiometrically adjusted patch $\bar{g}[.]$ is then used for the next optimization step. We use a linear transformation which can be written as $\bar{g}[\boldsymbol{u}] = \alpha + \beta\, g[\boldsymbol{u}]$, where $\boldsymbol{u}$ stands for the discrete image coordinates.

The general geometric transformation is denoted by $\boldsymbol{x} = \boldsymbol{\psi}(\boldsymbol{\xi}, \boldsymbol{u})$, transforming the image coordinates $\boldsymbol{u}$ to the parameter vector $\boldsymbol{\xi}$. Applying the least squares framework, this leads to

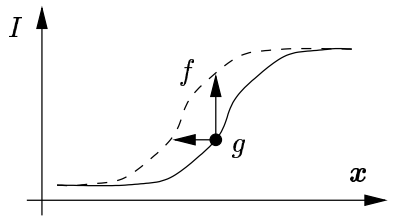

Figure 1: The ambiguity between radiometric and geometric transformation. Local operators cannot distinguish between the two types of transformations, hence a simultaneous estimation leads to an ill-conditioned system.

the observation equation

$$f[\boldsymbol{u}] + e[\boldsymbol{u}] = \bar{g}(\boldsymbol{x}) \,. \tag{1}$$

Equation (1) represents a relation between each greyvalue within the template and its corresponding image intensity in the search image. Notice that square brackets denote functions defined on a discrete grid. The functions $g(.)$ and $\bar{g}(.)$ simply represent the continuous versions of $g[.]$ and $\bar{g}[.]$, respectively. Hence, the template greyvalues $f[\boldsymbol{u}]$ are defined on the grid of the reference image while $\bar{g}(\boldsymbol{x}) = \bar{g}(\boldsymbol{\psi}(\boldsymbol{\xi}, \boldsymbol{u}))$ fall between the grid of the search image. Interpolating the greyvalues $\bar{g}(\boldsymbol{\psi}(\boldsymbol{\xi}, \boldsymbol{u}))$ for a given $\boldsymbol{\xi}$ we substitute

$$\tilde{g}_\xi[\boldsymbol{u}] := \bar{g}(\boldsymbol{\psi}(\boldsymbol{\xi}, \boldsymbol{u})) \,.$$

Based on a coordinate list $\boldsymbol{u}[k]$, equation (1) is reordered into a vector notation

$$\boldsymbol{f} + \boldsymbol{e} = \tilde{\boldsymbol{g}} \,, \tag{2}$$

building a series of n equations, where n is the number of pixels included in the template. Together with the least squares objective function $\boldsymbol{e^T P e}$, with $\boldsymbol{P}$ as optional weight matrix, this defines an unconstrained nonlinear least squares (NLS) problem.

We choose a Newton-Raphson scheme as optimization algorithm, linearizing the observation equation (1) around the current estimate $\boldsymbol{\xi}^\circ$ or $\boldsymbol{x}^\circ = \boldsymbol{\psi}(\boldsymbol{\xi}^\circ, \boldsymbol{u})$, respectively:

$$f[\boldsymbol{u}] + e[\boldsymbol{u}] = \bar{g}(\boldsymbol{x}^\circ) + \nabla_\xi \bar{g}(\boldsymbol{x}^\circ)\, \boldsymbol{\Delta\xi} \tag{3}$$

$$\boldsymbol{f} + \boldsymbol{e} = \tilde{\boldsymbol{g}}^\circ + \boldsymbol{A} \cdot \boldsymbol{\Delta\xi} \,, \tag{4}$$

where $\boldsymbol{A}$ is the Jacobian matrix with respect to the parameter vector $\boldsymbol{\xi}$. $\boldsymbol{A}$ is a $n \times r$ matrix with r being the number of parameters. If we neglect the stochastic nature of the Jacobian matrix, this linear problem corresponds to a Gauss-Markov model with full rank. Note that only under this assumption, the observations are separated from the parameters. Problem (4) is then solved analytically setting the first derivative of the least squares goal function $\boldsymbol{e^T P e}$ to zero, which yields the normal equation system

$$\boldsymbol{A^T P A} \cdot \boldsymbol{\Delta\xi} = -\boldsymbol{A^T P}\, (\tilde{\boldsymbol{g}}^\circ - \boldsymbol{f}) \tag{5}$$

$$\boldsymbol{N} \cdot \boldsymbol{\Delta\xi} = -\boldsymbol{A^T P}\, \boldsymbol{w} \,. \tag{6}$$

Notice that if $\boldsymbol{P}$ is a diagonal or a band-diagonal matrix, the matrix $\boldsymbol{A}$ doesn't have to be computed and stored as a whole. The weight matrix $\boldsymbol{P}$ is diagonal if and only if the observations are independent of each other. In the case of LSM, this assumption usually holds[1] and it is

[1] Strictly, the assumption is fulfilled only for the original observations f and g, and not for the transformed and interpolated patch $\tilde{g}$. But the influence of neglecting this becomes only significant for very high precision measurements.

sufficient to compute $\boldsymbol{A}$ row by row in order to build the normal matrix $\boldsymbol{N}$. This is an important property, since the size of $\boldsymbol{A}$ increases with the number of pixels included in the templates.

As long as $\boldsymbol{A}$ has no row deficiency, the $r \times r$ normal matrix $\boldsymbol{A^T P A}$ is always positive definite and symmetric and hence the Cholesky decomposition can be applied to solve equation (5). After each iteration step, matrix $\boldsymbol{A}$ must be recomputed using the updated set of parameters $\boldsymbol{\xi}^{t+1} = \boldsymbol{\xi}^t + \boldsymbol{\Delta\xi}$. When the parameter change $\boldsymbol{\Delta\xi}$ falls below a specified numerical resolution the iteration process is stopped.

Parameter estimation in linear least squares problems are extensively discussed in standard literature on parameter estimation theory, *e.g.*, [Koch 1988]. The iterative solution of equation (1) is an unbiased estimate for the unknowns with a stochastic variance expressed by the diagonal elements of the covariance matrix

$$\boldsymbol{\Sigma}_{\hat{\xi}\hat{\xi}} = \hat{\sigma}_0 \cdot \boldsymbol{Q}_{\hat{\xi}\hat{\xi}} \,. \tag{7}$$

The value $\hat{\sigma}_0$ denotes the a posteriori noise estimate and $\boldsymbol{Q}_{\hat{\xi}\hat{\xi}} = \boldsymbol{N^{-1}}$ is the cofactor matrix.

2.2 Affine transformation as geometric transformation

So far no assumptions have been made on the dimensionality of the problem and on what type of transformation is used. In the following, the case of a two dimensional affine transformation is presented. The corresponding parameter vector consists of six variables $\boldsymbol{\xi} = [t_1, t_2, m_1, s_1, s_2, m_2]^T$ and the coordinate transformation is written as

$$\boldsymbol{x} = \begin{bmatrix} t_1 \\ t_2 \end{bmatrix} + \begin{bmatrix} m_1 & s_1 \\ s_2 & m_2 \end{bmatrix} \boldsymbol{u} \,. \tag{8}$$

The derivative $\nabla_\xi \bar{g}(\boldsymbol{x})$ is now calculated explicitly using the chain rule. In vector notation, this leads to the $n \times 6$ Jacobian matrix $\boldsymbol{A}$ (cf. equation (4)), each line $\boldsymbol{A_k}$ representing the derivatives at $\boldsymbol{x}[k] = \boldsymbol{\psi}(\boldsymbol{\xi}, \boldsymbol{u}[k])$. Calculating the derivatives in the resampled patch image $\tilde{g}[.]$ and denoting the derivatives by $\tilde{g}_{u_1}[.]$ and $\tilde{g}_{u_2}[.]$, we write

$$\boldsymbol{A_k} = [\tilde{g}_{u_1},\ \tilde{g}_{u_2},\ \tilde{g}_{u_1}u_1,\ \tilde{g}_{u_1}u_2,\ \tilde{g}_{u_2}u_1,\ \tilde{g}_{u_2}u_2] \ ,$$

omitting the parameter $\boldsymbol{u}[k]$ of the functions $\tilde{g}_{u_i}[.]$ for better readability.

As mentioned in the previous section, the normal matrix $\boldsymbol{N} = \boldsymbol{A^T P A}$ can be built computing $\boldsymbol{A}$ row by row, as long as the weight matrix $\boldsymbol{P}$ is diagonal. If the greyvalues of each pixel are considered independent this is fulfilled and $\boldsymbol{N}$ is computed without the need to multiply large matrices.

2.3 Employing constraints

The least squares formalism allows one to introduce additional constraints in a simple and intuitive way. In addition to the observation equations, zero observations are included in the framework, which results in soft or spring constraints. In this section, we will apply this technique to LSM. As an examples serves the reduction of an affine to a similarity transformation. Instead of reparametrization we still employ equation (8) as transformation equation and add the following constraints to the parameter vector $\boldsymbol{\xi}$:

$$\begin{aligned} m_1 - m_2 + e_m &= 0 \\ s_1 + s_2 + e_s &= 0 \end{aligned}$$

Since $\boldsymbol{\xi}$ is not estimated directly, but only the parameter update $\boldsymbol{\Delta\xi}$, the derivative of these constraints must be taken analogous to the linearization of the observation equations. Thus, the matrix $\boldsymbol{A}$ is augmented by the constraint vectors

$$\begin{aligned} \boldsymbol{A_m} &= [0, 0, 1, 0, 0, -1] \\ \boldsymbol{A_s} &= [0, 0, 0, 1, 1, \ \ 0] \ . \end{aligned}$$

Employing constraints instead of reparametrization is easier to implement and also more versatile. On the one hand, constraints can easily be changed during the iteration, quickly switching from a similarity to an affine transformation. The formalism for the derivatives and therefore for building the normal matrix always stays the same. On the other hand, only a few types of constraints can actually be expressed by reparametrization, which makes constraints more flexible to use.

2.4 Multi template extension

There are several ways to extend the standard LSM to multiple templates. For all of them, the equation (1) has to be adapted to include multiple templates and their corresponding patches:

$$f^K[\boldsymbol{u}] + e^K[\boldsymbol{u}] = \bar{g}^K(\boldsymbol{x}^K) \,. \tag{9}$$

The most straightforward extension is to keep one single transformation for all patches $\boldsymbol{x}^K \equiv \boldsymbol{x}$ with the same parameter set shown in equation (8). The observations can be reordered into a vector notation analogous to the single template matching (2). Formally, this procedure is equal to the definition of one large template with several scattered regions of interest. The only difference is that the radiometric parameters α^K and β^K differ between the templates. Thus, the influence of bias fields and other global greyvalue errors is minimal.

2.5 Parameter determinability

The determinability of a parameter i is tested using its relative contribution δ_i to the trace of the cofactor matrix $\boldsymbol{Q}_{\hat{\xi}\hat{\xi}}$

$$\delta_i = \frac{\left|\mathrm{tr}[\boldsymbol{Q}_{\hat{\xi}\hat{\xi}}] - \mathrm{tr}[\boldsymbol{Q}^{\boldsymbol{i}}_{\hat{\xi}\hat{\xi}}]\right|}{\mathrm{tr}[\boldsymbol{Q}_{\hat{\xi}\hat{\xi}}]} \,, \tag{10}$$

where $\boldsymbol{Q}^{\boldsymbol{i}}_{\hat{\xi}\hat{\xi}}$ is the cofactor matrix with parameter i excluded. δ_i describes the influence of each parameter upon the others. Weakly determinable parameters cause quasi-singular normal equations, thus a large change in the trace of the cofactor matrix.

An efficient implementation of (10) is achieved by using the Kalman-Bucy filter technique (cf. [Koch 1988]), computing the partial cofactor matrix $\boldsymbol{Q}^{\boldsymbol{i}}_{\hat{\xi}\hat{\xi}}$ directly from $\boldsymbol{Q}_{\hat{\xi}\hat{\xi}}$. Applying this framework to (10) yields an expression for the contribution

$$\delta_i = \frac{\sum_j {q_{ij}}^2}{q_{ii} \sum_j {q_{jj}}^2} \,, \tag{11}$$

where q_{ij} denotes the elements of the full cofactor matrix $\boldsymbol{Q}_{\hat{\xi}\hat{\xi}}$.

If a contribution δ_i of the parameter i is high, this parameter strongly correlates to one or more parameters. One should either exclude parameter i or combine it with the correlating parameters by applying parameter constraints as described in section 2.3.

3 Controlling patient position in radiotherapy

The steps before high precision conformal therapy include the acquisition of a CT, then a 3D planning of beam directions, field shape and dose distribution and finally the positioning of the patient using a simulator with the same geometry as the linear accelerator (figure 2). During the radiotherapy treatment, either portal films or electronic portal images are acquired for quality control.

The portal images in this work were acquired at the University Hospital of Zürich using a Varian accelerator and their electronic portal imaging device (EPID). This device delivers a

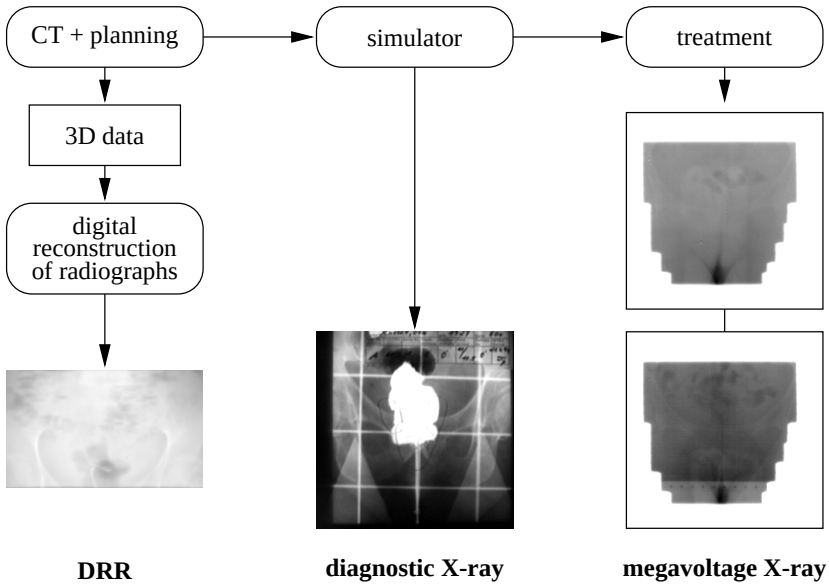

Figure 2: Overview of the different steps of radiotherapy treatment.

distortion free image with a resolution of 256×256 pixel on an area of 32×32 cm^2 [van Herk and Meertens 1988].

The diagnostic X-ray images from the simulator are often used as a reference image for measuring the patient motion in subsequent portal images. One goal of this project is to eliminate the need for simulator X-ray images for motion measurements by direct comparison with the DRR. Besides the fact that simulator images are not suitable for automated area-based matching due to their different greyvalue characteristics, they also represent an additional source of error with respect to the original planning data. Moreover, it is thus conceivable to circumvent the step of therapy simulation entirely in order to increase safety and to save costs. DRRs are employed in two ways:

1. One reference image is computed representing the optimum patient position. Subsequent portal images are compared against this reference image and the estimate of a 2D affine transformation leads to a correction of the patient position.

2. Each portal image is compared against a series of DRRs, including minor out-of-plane rotations to better account for the 3D patient motion.

In order to compute DRRs with sufficient quality, the CT slice thickness should be no larger than 3 mm.

3.1 Template selection

In the particular problem of portal images, two displacements must be computed. Since the EPID is in general not in a fixed position, a common coordinate system must be established using the edges of the radiation field. These edges are very distinct features and pose no problems to the matching algorithm. We refer to [Berger and Danuser 1997] for a more detailed description of the fieldedge match.

In the following, we will concentrate on the anatomy match. The selection of the template regions strictly follows the previous work. Due to artifacts and the presence of distinct but unstable features (*e.g.*, originating from air in the rectum), a fully automated template selection is beyond the possibilities of computer vision. Thus, the physician has to position predefined standard templates onto the significant structures in the reference image.

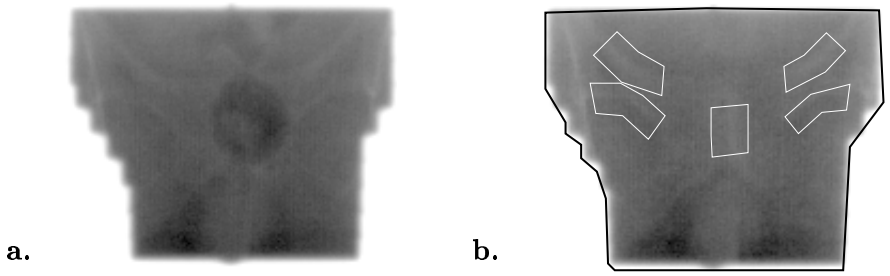

Figure 3: Image (a) depicts a portal image with a common unstable features that originates from air in the rectum (dark blur in the center of the image). A typical template selection for a AP pelvis field is shown in (b).

3.2 Self-diagnosis within LSM

We first focus on the determinability analysis as described in section 2.5. Since the statistics behind the self-diagnosis is valid only in the adjusted state, this measure can not be applied directly to the initial system. However, an upper bound for the determinability is computed matching the templates onto themselves.

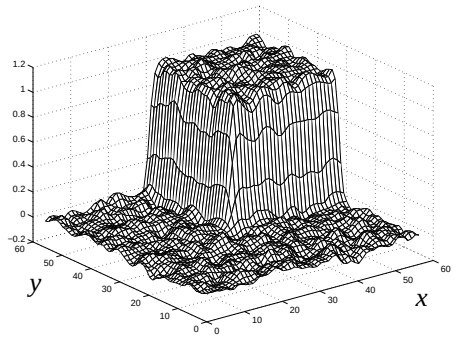

$$\begin{bmatrix} \delta_{m_1} & \delta_{s_1} \\ \delta_{s_2} & \delta_{m_2} \end{bmatrix} = \begin{bmatrix} 0.4424 & 0.0922 \\ 0.0958 & 0.3731 \end{bmatrix}$$

Figure 4: Mesh view of the test image for the determinability analysis. Based on a match onto itself, the contribution values of all parameter are computed. As expected, the contribution of the scale parameters δ_{m_i} is significantly higher than of the shear parameters δ_{s_i}.

The example in figure 4 illustrates the meaning of the contribution values. The 63×63 test image contains a noisy corner with a signal to noise ratio of 10. It is Gaussian filtered with $\sigma = 1$. Building the normal equation system by matching the template onto itself, the contribution values shown in figure 4 result. As expected, the contribution of the scale parameters is significantly higher than of the shear parameters, which clearly reveals the weak determinability of the two scale parameters.

A suitable matching strategy is to estimate a congruent transformation first and then to test the full affine parameter set for determinability. If none of them shows intolerably large contributions δ, the optimization is continued with the full parameter set. A general flowchart is depicted in figure 5.

The cross-correlation between the template $f[.]$ and the patch $\tilde{g}[.]$ — which is interpolated from the search image using the final parameter set $\boldsymbol{\xi}$ — should be very close to 1.0. If the correlation coefficient is below a certain threshold, the analysis of the final error vector $\boldsymbol{e}$ might point at an incorrectly aligned template. Large values of $\boldsymbol{e}$ indicate a mismatch for this region. Excluding such a template and reoptimizing the geometric transformation may result in a better parameter set.

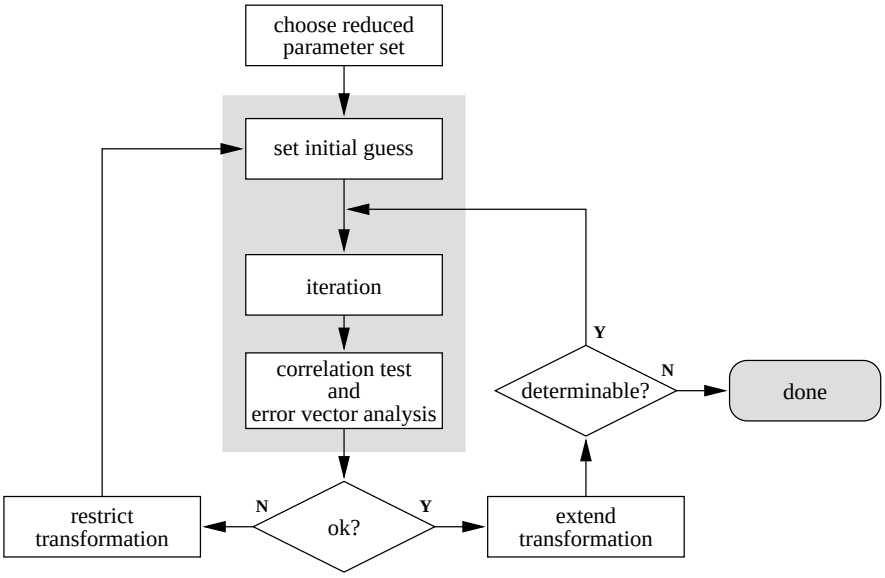

Figure 5: Flowchart of the diagnostic measures.

3.3 Combine multiple 2D measurements to 3D motion estimate

In radiotherapy, the patient is treated from different directions during one treatment session. In the case of prostate cancer treatment for example, the four directions AP, PA, 90°, 270° are typical (figure 6). Even though images from different directions are matched separately, the 2D results combine to a rough 3D motion estimate. In the near future, this combination will help to validate and possibly to improve the measurements.

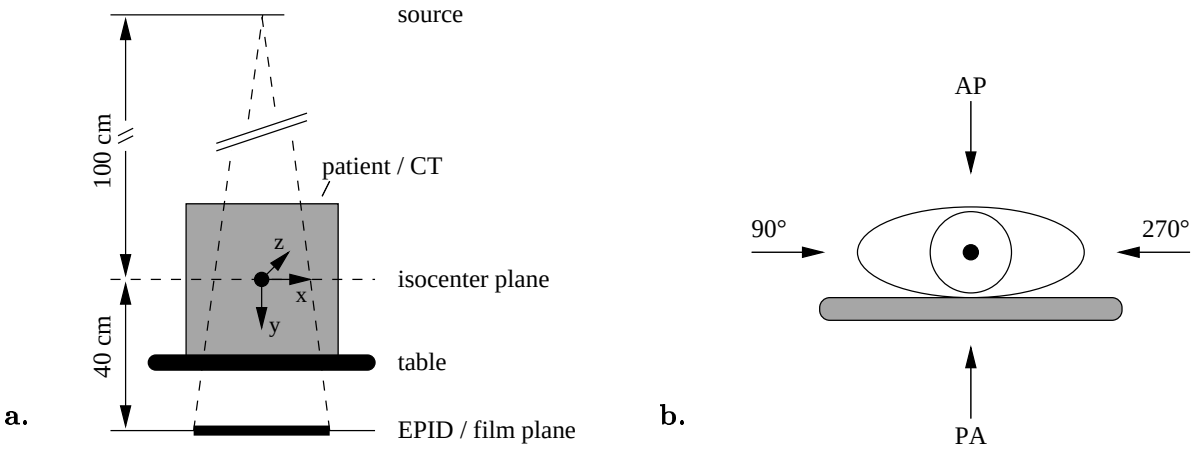

Figure 6: The therapy setup is illustrated in (a) including the patient coordinate system. The four main beam directions are shown in (b).

4 Results

The high precision capabilities of LSM are extensively shown in [Berger and Danuser 1997, Danuser and Mazza 1996, Danuser 1996]. In the following sections, the emphasis is on the estimation of the in-plane part of the 3D patient motion based on the evaluation of projected 2D images. We first apply the algorithm to generated datasets to test the potential of LSM. In the last section, we present preliminary tests of the multi-modal match.

4.1 In-plane translation and rotations

The following test series consisted of 25 simulated portal images with a maximum patient displacement of 20 mm in x and y direction and a maximum rotation of 10° (figure 7). The results are depicted in figure 9 a. The standard deviations of the translation measurements are 0.25 pixel (0.23 mm) in x direction and 0.37 pixel (0.33 mm) in y direction. These systematic errors are caused by the unknown y position in the CT coordinate system of the template features (see figure 6 for an illustration of the CT coordinate system). Within the rotation measurement, these systematic error do not occur and the standard deviations are below 0.01°.

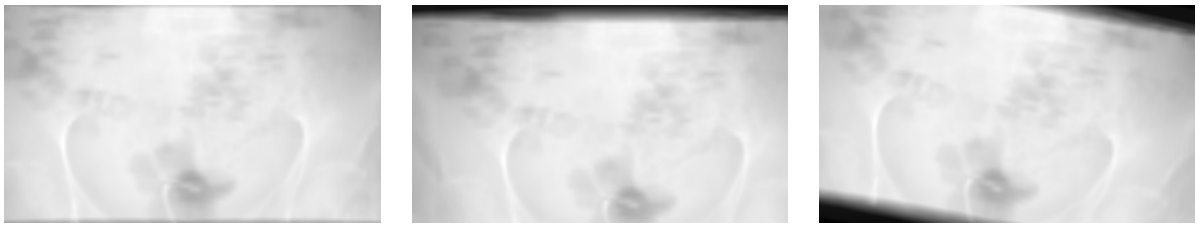

a. reference image **b.** 25 translated images **c.** 10 rotated images

Figure 7: In-plane test series computed from CT volume. The CT is translated and rotated in the image plane.

4.2 Including out-of-plane rotation

In order to test under more realistic conditions, a test series with small out-of-plane rotations is generated (figure 8). The area-based match still finds the corresponding regions with a correlation well above 0.9. The systematic errors already encountered in the example above, which are an inherent problem of using projected images, are of course higher in this example. But the total point errors of 1.24 mm for 2° rotation and 3 mm for 5° still are promising results (see figure 9 b).

a. reference image **b.** 100 images rotated around x axis **c.** 100 images rotated around z axis

Figure 8: Out-of-plane rotation test series computed from CT volume.

4.3 Multi-modal match with portal images

The CT data acquired for radiotherapy in the current hospital routine consists of 10 mm slices, which is too coarse for an accurate computation of DRRs. At the moment, only one — unfortunately incomplete — data set with 3 mm slicing is available. Better datasets are acquired in the near future. Thus, no tests for measuring a full 2D affine transformation could be carried out. Nevertheless, the results on measuring translation and scale are promising. Figure 10 a shows the partly reconstructed radiograph with the chosen templates and two validation lines. The matching results to two portal images are depicted in 10 b and c.

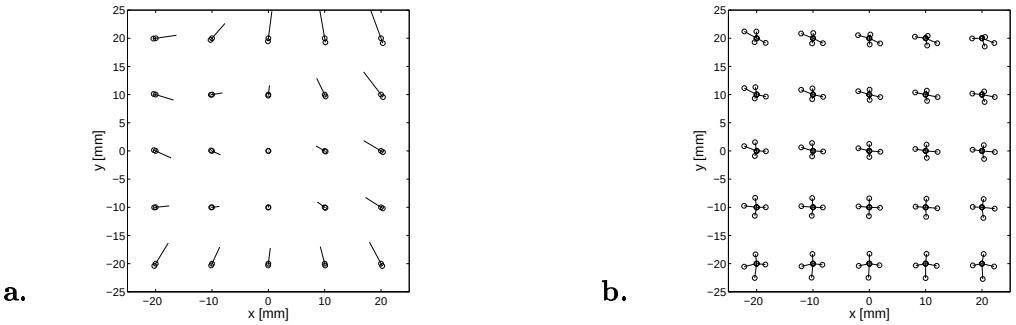

Figure 9: Displacement measure errors in test series without (a) and including out-of-plane rotations of 2° (b). In (a) the error vectors are enlarged by a factor 10. The total point error amounts to 0.3 pixel (0.28 mm) without and 1.4 pixel (1.25 mm) with out-of-plane rotations.

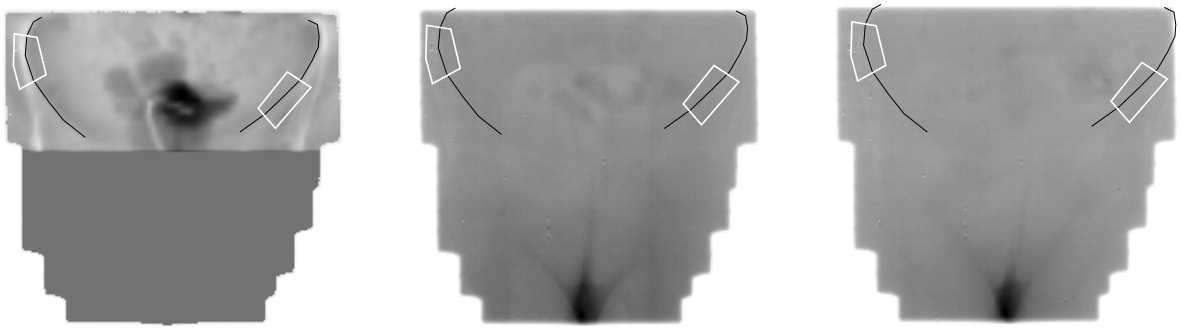

a. reference image

b. translation (2,-1) mm
scale 1.05

c. translation (7,-2) mm
scale 1.06

Figure 10: Multi-modal match between a DRR image computed from incomplete CT data (a) and a portal image series (b,c). The transformation model includes translation and scale. The white polygons outline the template regions and patches respectively, the black lines represent validation lines which are not used for matching.

5 Conclusion and Outlook

The LSM method with deformable template regions is a versatile matching algorithm. Since it is an area-based method, the often unreliable step of feature extraction is circumvented. Especially in low-contrast imagery like megavoltage X-ray images (portal images), this is an important feature.

In earlier work, LSM has been successfully applied to matching megavoltage X-ray images of the same modality. The results presented in this paper show the suitability for a multi-modal match between digitally reconstructed radiographs as reference images and the portal images acquired during radiotherapy. The area-based method LSM proved robustness even when matching slightly distorted patterns.

In two test series with generated data, the systematic error caused by estimating a 3D motion from projected 2D images is examined. Furthermore, preliminary tests with an incomplete DRR matched to real portal images show promising results. A complete data set will be available soon and allow for a full test of the multi-modal displacement measurements. Another goal is to combine multiple 2D measurements to better estimate the 3D motion as outlined in section 3.3. Thus, the influence of the systematic error occurring in the 2D measurements is reduced.

The presented methods are a step further in the direction of automatically controlling the patient position in radiotherapy. Applied in daily hospital routine, this should lead to an improved quality assurance in radiotherapy.

Acknowledgments. We would like to thank Dr. U. R. Meier and Prof. Dr. U. M. Lütolf for providing the portal images and useful information concerning medical topics. This work was granted by the Swiss Cancer League and the Walter Honegger Foundation.

References

[Bergen *et al.* 1992] J. R. Bergen, P. Anandan, K. J. Hanna, and R. Hingorani. Hierarchical Model-Based Motion Estimation. In G. Sandini, editor, *Computer Vision ECCV'92*, pages 237–252, Santa Margherita Ligure, Italy, 1992. Springer.

[Berger and Danuser 1997] Martin Berger and Gaudenz Danuser. Deformable Multi Template Matching with Application to Portal Images. In *Proceedings Computer Vision and Pattern Recognition '97*, pages 374–379. IEEE Computer Society Press, 1997.

[Berger 1998] Martin Berger. The framework of least squares template matching. Technical Report 180, Image Science Lab, ETH Zürich, 1998.

[Danuser and Mazza 1996] G. Danuser and E. Mazza. Observing Deformations of 20 Nanometer with a Low Numerical Aperture Light Microscope. In C. Gorecki, editor, *Optical Inspection and Micromeasurements*, volume 2782, pages 180–191. European Optical Society, SPIE, 1996.

[Danuser 1996] G. Danuser. Stereo Light Microscope Calibration for 3D Submicron Vision. In K. Kraus and P. Waldhäusl, editors, *Proceedings of the 18th ISPRS Congress*, volume 31/B5, pages 101–108, Vienna, Austria, July 1996. ISPRS.

[Dong and Boyer 1996] L. Dong and A. L. Boyer. A portal image alignment and patient setup verification procedure using moments and correlation techniques. *Phys. Med. Biol.*, 41(4):697–723, April 1996.

[Förstner 1987] W. Förstner. Reliability analysis of parameter estimation in linear models with applications to mensuration problems in computer vision. *Computer Vision, Graphics, and Image Processing*, 40:273–310, 1987.

[Fritsch *et al.* 1995] D. S. Fritsch, E. L. Chaney, A. Boxwala, M. McAuliffe, S. Raghavan, A. Thall, and J. R. D. Earnhart. Core-based Portal Image Registration for Automatic Radiotherapy Treatment Verification. *Int'l J. Radiation Oncology Biol. Phys.*, 33(5):1287–1300, 1995.

[Gilhuijs and van Herk 1993] K. G. A. Gilhuijs and M. van Herk. Automatic on-line inspection of patient setup in radiation therapy using digital portal images. *Med. Phys.*, 20(3):667–677, 1993.

[Grün 1985] A. Grün. Adaptive Least Squares Correlation: A Powerful Image Matching Technique. *South African Journal of Photogrammetry, Remote Sensing & Cartography*, 14(3):175–187, 1985.

[Koch 1988] K. R. Koch. *Parameter Estimation and Hypothesis Testing in Linear Models.* Springer, 1988.

[Lindeberg 1995] T. Lindeberg. Direct estimation of affine image deformations using visual front-end operations with automatic scale selection. In *Fifth International Conference on Computer Vision ICCV'95*, pages 134–141, Cambridge, MA, 1995. IEEE Computer Society Press.

[Lucas and Kanade 1981] Bruce D. Lucas and Takeo Kanade. An Iterative Image Registration Technique with an Application to Stereo Vision. In *International joint conference on artificial intelligence*, pages 674–679, 1981.

[Moseley and Munro 1994] J. Moseley and P. Munro. A semiautomatic method for registration of portal images. *Med. Phys.*, 21(4):551–558, April 1994.

[Radcliffe *et al.* 1994] T. Radcliffe, R. Rajapakshe, and S. Shalev. Pseudocorrelation: A fast, robust, absolute, grey-level image alignment algorithm. *Med. Phys.*, 21(6):761–769, June 1994.

[Unser *et al.* 1995] M. Unser, P. Thévenaz, L. Chulhee, and U. Ruttimann. Registration and Statistical Analysis of PET Images Using the Wavelet Transform. *IEEE Engineering in Medicine and Biology*, September/October 1995.

[van Herk and Meertens 1988] M. van Herk and H. Meertens. A matrix ionisation chamber imaging device for on-line patient setup verification during radiotherapy. *Radiother. Oncol.*, 11(4):369–378, April 1988.